# Reactions of $SO_3$ with the O/H Radical Pool under Combustion Conditions†

**Lusi Hindiyarti and Peter Glarborg***

*Department of Chemical Engineering, Technical University of Denmark, DK-2800 Lyngby, Denmark*

**Paul Marshall**

*Center for Advanced Scientific Computation and Modeling, Department of Chemistry, University of North Texas, P.O. Box 305070, Denton, Texas 76203-5070*

*Received: November 13, 2006; In Final Form: January 25, 2007*

The reactions of $SO_3$ with H, O, and OH radicals have been investigated by ab initio calculations. For the $SO_3 + H$ reaction (1), the lowest energy pathway involves initial formation of $HSO_3$ and rearrangement to $HOSO_2$, followed by dissociation to $OH + SO_2$. The reaction is fast, with $k_1 = 8.4 \times 10^9 T^{1.22} \exp(-13.9 \text{ kJ mol}^{-1}/RT)$ cm$^3$ mol$^{-1}$ s$^{-1}$ (700−2000 K). The $SO_3 + O \rightarrow SO_2 + O_2$ reaction (2) may proceed on both the triplet and singlet surfaces, but due to a high barrier the reaction is predicted to be slow. The rate constant can be described as $k_2 = 2.8 \times 10^4 T^{2.57} \exp(-122.3 \text{ kJ mol}^{-1}/RT)$ cm$^3$ mol$^{-1}$ s$^{-1}$ for $T > 1000$ K. The $SO_3 + OH$ reaction to form $SO_2 + HO_2$ (3) proceeds by direct abstraction but is comparatively slow, with $k_3 = 4.8 \times 10^4 T^{2.46} \exp(-114.1 \text{ kJ mol}^{-1}/RT)$ cm$^3$ mol$^{-1}$ s$^{-1}$ (800−2000 K). The revised rate constants and detailed reaction mechanism are consistent with experimental data from batch reactors, flow reactors, and laminar flames on oxidation of $SO_2$ to $SO_3$. The $SO_3 + O$ reaction is found to be insignificant during most conditions of interest; even in lean flames, $SO_3 + H$ is the major consumption reaction for $SO_3$.

## Introduction

High-temperature sulfur reactions continue to be of both theoretical and practical interest.[1] The combustion of fuel-bound sulfur results in formation of oxides of sulfur, mainly $SO_2$ and $SO_3$. Sulfur trioxide in combustion systems causes formation of sulfuric acid, which will condense and corrode metal surfaces at temperatures below the dew point.[2,3] In addition, it may contribute to aerosols and particulate emissions.[4−6] A better understanding of the mechanisms for $SO_3$ formation and destruction is a necessary step in the effort to minimize these problems. A number of reactions may conceivably affect the $SO_3$ concentration. Reactions of particular interest are those of $SO_3$ with H, O, and OH,

$$SO_3 + H \rightleftharpoons SO_2 + OH \quad (1)$$

$$SO_3 + O \rightleftharpoons SO_2 + O_2 \quad (2)$$

$$SO_3 + OH \rightleftharpoons SO_2 + HO_2 \quad (3)$$

Depending on the reaction conditions, these steps may serve to either consume $SO_3$ (forward direction) or form $SO_3$ (reverse direction). Another important reaction for the $SO_3/SO_2$ ratio is the pressure-dependent step,

$$SO_2 + O(+M) \rightleftharpoons SO_3(+M) \quad (4)$$

Under the excess oxygen conditions typical of the post-flame region in a combustion system it is believed that the $SO_3/SO_2$ ratio is mainly controlled by the sequence (4), (2),[2,7−10] whereas reactions 1 and 3 presumably are less important. Although the $SO_3$ formation step (4) is characterized over a wide temperature and pressure range,[11,12] there is a significant uncertainty in the rate constants for the consumption reactions (1)−(3). There are no reported measurements for the $SO_3 + H$ reaction; kinetic models for sulfur chemistry rely on estimated values for $k_1$[13−15] or adopt a QRRK estimate[7] for the reverse reaction $SO_2 + OH$.[10,16,17] The rate constant for the reaction between $SO_3$ and O (2) has not been measured directly and reported data vary by several orders of magnitude. Indirect determinations have been reported on the basis of results from laminar premixed flames[18−22] and, for the reverse step, from reactor experiments.[10,23] A recent re-interpretation of selected flame results,[12] based on a more accurate value of $k_4$, indicates a fairly high rate constant for reaction $SO_3 + O \rightleftharpoons SO_2 + O_2$, in agreement with earlier evaluations,[20−22] and a fast reaction is also supported by other experiments.[18,19,23] In conflict with these results, Alzueta et al.[10] recommend a very low rate constant, which indicates that the reaction is insignificant under most conditions of interest. In the absence of measurements, the $SO_3 + OH$ reaction (3) has been omitted from most previous modeling studies of sulfur chemistry,[7,10,14−16] but it is potentially an important step.

The objective of the present work is to use ab initio calculations to obtain reliable estimates for the reactions of $SO_3$ with H, O, and OH. A recent reaction mechanism for sulfur chemistry[17] is updated with the new values for $k_1$, $k_2$, and $k_3$, and predictions with the revised model are compared to a range of experimental results from literature on the oxidation of $SO_2$ to $SO_3$. Finally, the implications for modeling the $SO_3/SO_2$ ratio in practical combustion systems are outlined.

## Ab Initio Calculations

**Computational Methodology.** The geometries of reactants, bound minima, products, and connecting transition states (TSs) were derived with the B3LYP level of density functional theory

† Part of the special issue "James A. Miller Festschrift".

10.1021/jp067499p CCC: $37.00 
Published on Web 03/09/2007

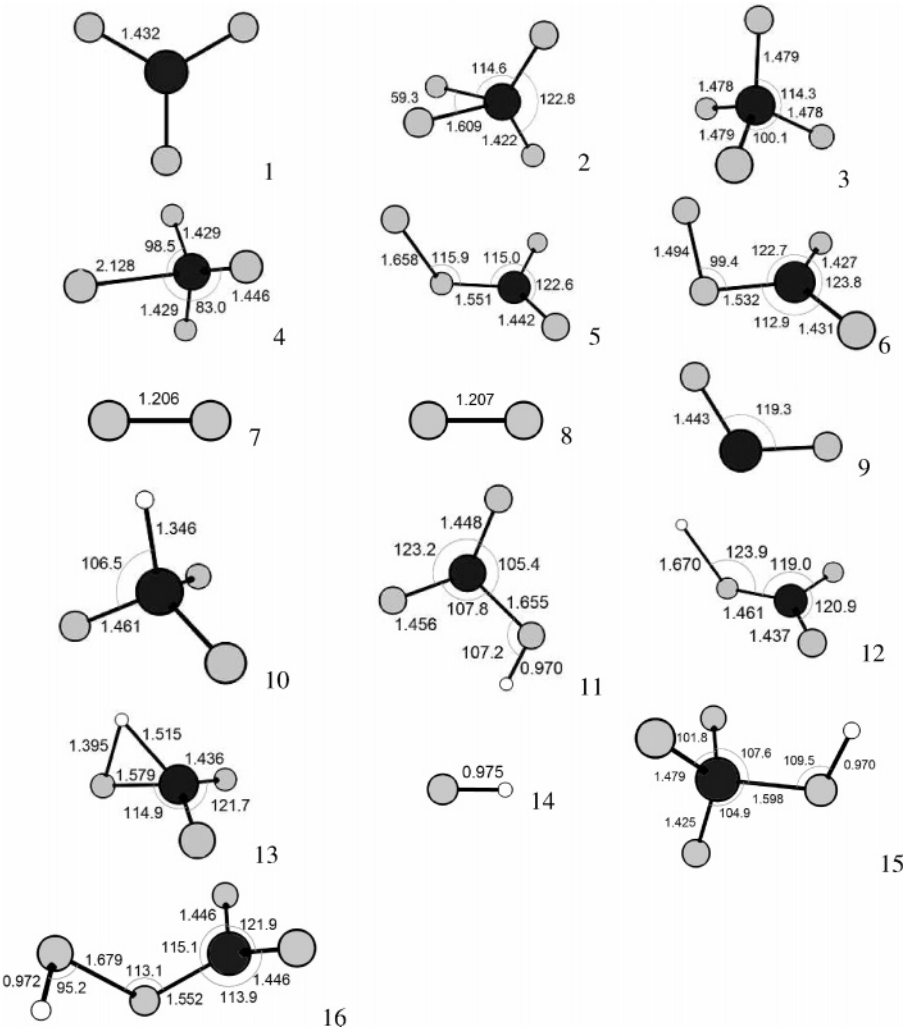


**Figure 1.** Computed B3LYP/6-311G(2d,d,p) geometries (distances in $10^{-10}$ m and angles in degrees): 1, $D_{3h}$ $SO_3$ $^1A_1'$; 2, $C_{2v}$ $SO_4$ $^1A_1$; 3 $C_{2v}$ $SO_4$ $^3A_2$; 4, $C_s$ TS1 $^3A''$; 5, $C_{2v}$ TS2 $^3A''$; 6, $C_1$ TS3 $^1A$; 7, $O_2$ $^3\Sigma$; 8, $^1O_2$; 9, $C_{2v}$ $SO_2$ $^1A_1$; 10, $C_{3v}$ $HSO_3$ $^2A_2$; 11, $C_1$ $HOSO_2$ $^2A$; 12, $C_s$ TS4 $^2A'$; 13, $C_s$ TS5 $^2A'$; 14, OH $^2\Pi$; 15, $HOSO_3$ $^2A''$; 16, $C_1$ TS6 $^2A$.

**TABLE 1: CBS-QB3 Energies (0 K, in au; 1 au = 2625.5 kJ mol$^{-1}$) and B3LYP/6-311G(2d,d,p) Vibrational Frequencies (cm$^{-1}$, Scaled by 0.99) Computed for the Reactants, Intermediates, Products, and Transition States in the H, O, and OH Reactions with $SO_3$ Shown in Figure 1**

| molecule | energy, au | frequencies, cm$^{-1}$ |
|---|---|---|
| O $^3$P | −74.98763 | |
| $SO_3$ $^1A_1'$ | −623.15539 | 488, 508, 508, 1034, 1350, 1350 |
| $SO_4$ $^1A_1$ | −698.18631 | 299, 464, 465, 480, 635, 654, 895, 1224, 1403 |
| $SO_4$ $^3A''$ | −698.17571 | 299, 350, 384, 384, 438, 779, 780, 941, 1159 |
| TS1 $^3A''$ | −698.14226 | 214i, 125, 130, 469, 494, 499, 1022, 1267, 1346 |
| TS2 $^3A''$ | −698.09006 | 897i, 96, 167, 436, 461, 511, 748, 1114, 1303 |
| TS3 $^1$A | −698.09604 | 530i, 142, 286, 412, 468, 654, 841, 1177, 1376 |
| $O_2$ $^3\Sigma$ | −150.16462 | 1625 |
| $^1O_2$ | −150.11901 | 1611 |
| $SO_2$ $^1A_1$ | −548.03762 | 508, 1141, 1335 |
| $HSO_3$ $^2A_2$ | −623.68528 | 178, 178, 567, 944, 944, 1039, 1104, 1104, 2580 |
| $HOSO_2$ $^2$A | −623.73026 | 262, 399, 405, 507, 679, 1059, 1105, 1265, 3715 |
| TS4 $^2A'$ | −623.63844 | 975i, 178, 297, 490, 498, 550, 977, 1255, 1334 |
| TS5 $^2A'$ | −623.64774 | 1486i, 406, 463, 525, 643, 775, 1139, 1334, 1887 |
| OH $^2\Pi$ | −75.64969 | 3668 |
| H $^2$S | −0.49982 | |
| $HOSO_3$ $^2A''$ | −698.85077 | 214, 266, 361, 408, 429, 522, 791, 840, 1022, 1150, 1240, 3724 |
| TS6 $^2$A | −698.75939 | 745i, 87, 175, 243, 444, 469, 515, 743, 1082, 1102, 1281, 3711 |

combined with the 6-311G(2d,d,p) basis set.[24] These results are shown in Figure 1. Vibrational frequencies at the same level of theory were scaled by a standard factor of 0.99[24] and are listed in Table 1. For thermochemistry calculations, all internal motions were treated as harmonic oscillators, with the usual assumption of separability of rotations and vibrations. Improved single-point energies were obtained with the CBS-QB3 composite approach of Petersson and co-workers, which approximates CCSD(T) calculations extrapolated to the infinite basis set limit and has been shown to give atomization energies

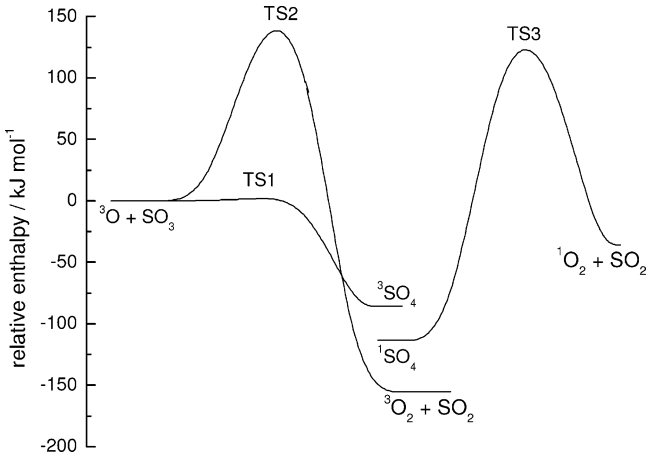


**Figure 2.** Potential energy diagram for $O + SO_3$ based on CBS-QB3 calculations, showing relative enthalpies at 0 K.

with mean absolute deviation of 2.4 kJ mol$^{-1}$.[24] Simple transition state theory (TST) was applied to obtain rate constants $k$, in the form

$$k = \frac{k_B T}{h} \frac{Q_{TS}}{Q_{reactants}} \exp(-E_0/RT)$$

where the partition functions $Q$ and the 0 K energy barriers $E_0$ were derived from the CBS-QB3 data.

**$SO_3$ + O Reaction.** The potential energy diagram is shown in Figure 2. Several states of $SO_4$ have been investigated in the past,[25,26] which arise from symmetry breaking in tetrahedral $SO_4$. Here we focus on the lowest energy singlet and triplet states. Direct abstraction to form $^3O_2 + SO_2$ via TS2 is found to have a high barrier of 139 kJ mol$^{-1}$. The computed $\Delta_r H_0$ is $-155.5$ kJ mol$^{-1}$, which compares well with the JANAF evaluation of $-151.1 \pm 0.7$ kJ mol$^{-1}$.[27] TST yields a rate constant of $4.1 \times 10^7 T^{1.71} \exp(-138.1 \text{ kJ mol}^{-1}/RT)$ cm$^3$ mol$^{-1}$ s$^{-1}$ for $T > 1000$ K. In contrast, spin-allowed addition via TS1 to form triplet $SO_4$ is predicted to occur with a small barrier of only 2 kJ mol$^{-1}$. This low barrier may be consistent with the experiments over 300−500 K of Westenberg and de Haas,[28] who argued in favor of pressure-dependent adduct formation (they did not observe $SO_4$ by mass spectrometry. Possibly the adduct decomposed before or during ionization). The computed bond dissociation enthalpy at 0 K, $D_0(O-SO_3) = 85.8$ kJ mol$^{-1}$, implies $\Delta_f H_0(^3SO_4) = -229.0$ kJ mol$^{-1}$, with an uncertainty of around 5 kJ mol$^{-1}$. However, at combustion temperatures this triplet adduct will not be thermodynamically stable. We have not been able to find a reaction path for the spin-allowed dissociation of $^3SO_4$ to $^3O_2 + SO_2$, but intersystem crossing to the somewhat more stable singlet $SO_4$ (predicted $\Delta_f H_0(^1SO_4) = -256.8$ kJ mol$^{-1}$) may be possible, especially if collisionally assisted. Spin-allowed dissociation of this singlet adduct to $^1O_2 + SO_2$ via TS3 has a computed barrier of 123 kJ mol$^{-1}$. Treatment of this step as the bottleneck with the assumption that $^1SO_4$ is in rapid equilibrium with the reactants via TST leads to a rate constant of $1.1 \times 10^7 T^{1.55} \exp(-120.5 \text{ kJ mol}^{-1}/RT)$ cm$^3$ mol$^{-1}$ s$^{-1}$ for $T > 1000$ K. The single-reference CBS-QB3 energy for $^1O_2 + SO_2$ is poorly defined because singlet oxygen is a multireference species. The experimental 0 K enthalpies of $SO_2$ with $O_2$ in the a $^1\Delta_g$, b $^1\Delta_g^+$, and c $^1\Sigma_u$ states, relative to the reactants, are $-56.8$, $-5.8$, and 239.6 kJ mol$^{-1}$.[27] As expected, these values bracket the computed $\Delta_r H_0$ of $-36$ kJ mol$^{-1}$, which presumably corresponds to some combination of the singlet states of $O_2$. Multireference studies of this pathway may be needed.

**TABLE 2: B3LYP/aug-cc-pV(T+d)Z Energies (Including Zero Point Energies) for Stationary Points on the $O + SO_3$ Potential Energy Surface and Enthalpies at 0 K Relative to Reactants**

| species | B3LYP energy (au) | B3LYP enthalpy (kJ/mol) | CBS-QB3 enthalpy (kJ/mol) |
|---|---|---|---|
| $^3O$ | −75.09418 | 0 | 0 |
| $SO_3$ | −623.93744 | | |
| $O_2$ | −150.38092 | −180 | −155, −151[a] |
| $SO_2$ | −548.71939 | | |
| $^3SO_4$ | −699.07583 | −116 | −86 |
| $^1SO_4$ | −699.06654 | −92 | −114 |
| TS1 | −699.03623 | −12 | 2 |
| TS2 | −698.99222 | 103 | 139 |
| TS3 | −698.98777 | 115 | 123 |
| $^1O_2$ | −150.34887[b] | −87[c] | −36,[c] −57[a,c] |

[a] Experiment.[27] [b] Corrected spin-unrestricted result (see text). [c] Includes $SO_2$.

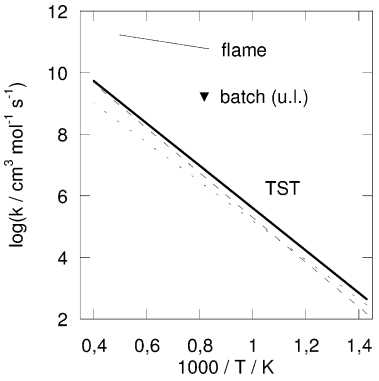


**Figure 3.** Arrhenius plot for the $SO_3 + O$ reaction. Thin solid line: the rate constant derived by Yilmaz et al.[12] based on flame measurements.[20,21,22] Solid triangle: upper limit (ref 10, present work) based on batch reactor data.[31] Long-dashed line: TST for $O + SO_3$ triplet abstraction. Short-dashed line: TST for $O + SO_3$ singlet addition/elimination. Thick solid line: TST total rate constant.

An alternative approach is based on density functional theory (DFT). For comparison, we reoptimized the $O + SO_3$ stationary points at the B3LYP/aug-cc-pV(T+d)Z level of theory, where the basis set includes tight d functions on sulfur.[29] The energies, including unscaled zero point vibrational energies, are summarized in Table 2. For singlet oxygen, the spin-restricted wavefunction is unstable with respect to becoming spin-unrestricted, with an expectation value for the spin operator, $\langle S^2 \rangle$, equal to 1.005. An improved estimate of the $^1O_2$ energy that corrects for spin contamination is obtained via the procedure of Yamaguchi et al.,[30] and the result is shown in Table 2. The derived $^3\Sigma - ^1\Delta$ gap for $O_2$ is 84 kJ mol$^{-1}$, in good accord with the experimental value of 95 kJ mol$^{-1}$.[27] For the other singlet species, the spin-restricted DFT results were stable with respect to relaxation of spin constraints, although this does not rule out some multireference character in the wavefunctions. As may be seen from the relative enthalpies shown in Table 2, the DFT results underestimate $\Delta H_0$ for O-atom abstraction from $SO_3$ by about 30 kJ mol$^{-1}$. DFT yields lowered reaction barriers, by 8−36 kJ mol$^{-1}$. DFT also reverses the order of singlet and triplet states for $SO_4$ by comparison with CBS-QB3 theory. A singlet ground state was obtained by McKee[25] and, until multireference calculations are available, we prefer CBS-QB3 data for the transition state theory analysis.

The singlet and triplet paths have similar rate constants above 1000 K, as may be seen in Figure 3. The current recommendation for $k_2$ is the sum of both channels, $k_2 = 2.8 \times 10^4 T^{2.57} \exp(-122.3 \text{ kJ mol}^{-1}/RT)$ cm$^3$ mol$^{-1}$ s$^{-1}$. It is several

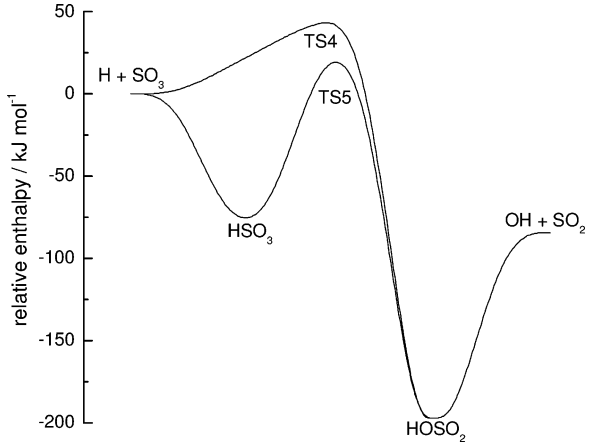


**Figure 4.** Potential energy diagram for $H + SO_3$ based on CBS-QB3 calculations, showing relative enthalpies at 0 K.

orders of magnitude lower than values derived from flames,[12,20−22] but a low value is in agreement with the recommendation of Alzueta et al.[10] based on batch reactor data.[31] The flame and batch reactor results are discussed further below.

**$SO_3$ + H Reaction.** Two bound minima, corresponding to formation of an S−H or an O−H bond by H-atom addition, were characterized and are shown in Figure 4. TSs were found for both addition processes and, like in the analogous $H + SO_2$ system,[32] formation of the less strongly bound $HSO_3$ species is more kinetically favorable than formation of the more thermodynamically stable $HOSO_2$ molecule. Isomerization between these addition products is also possible and is important because the lowest energy pathway on Figure 4 involves initial formation of $HSO_3$ followed by rearrangement to $HOSO_2$, followed by dissociation to $OH + SO_2$. As a check on the accuracy of the CBS-QB3 energies, we compute $\Delta_r H_0$ for the overall reaction to be −84.5 kJ mol$^{-1}$, which compares well with the experimental value of −83.2 kJ mol$^{-1}$, which is based on JANAF data[27] except for OH.[33]

The predicted binding enthalpies of the adducts at 0 K are $D_0(H-SO_3) = 79.1$ kJ mol$^{-1}$ and $D_0(H-OSO_2) = 197.2$ kJ mol$^{-1}$, respectively. The corresponding $\Delta_f H_0$ are −253.1 and −371.2 kJ mol$^{-1}$, respectively, and the computed $\Delta_f H_{298}(HOSO_2) = -379.2$ kJ mol$^{-1}$ agrees with $-373 \pm 6$ kJ mol$^{-1}$ measured by Pilling and co-workers based on the $OH + SO_2$ equilibrium.[34] At low temperatures $HSO_3$ could be a sink for H atoms, but this molecule is not stable at high temperatures. We found no barrier for the initial addition $H + SO_3 \rightarrow HSO_3$ and the bottleneck in the overall reaction will be at TS5. This controls isomerization to $HOSO_2$ which, being created with an internal energy well in excess of the threshold for $OH + SO_2$ production (see Figure 4), is expected to dissociate immediately. TS5 was analyzed via TST for the temperatures of interest, 700−2000 K, and the results may be summarized as $k = 8.4 \times 10^9 T^{1.22} \exp(-13.9 \text{ kJ mol}^{-1}/RT)$ cm$^3$ mol$^{-1}$ s$^{-1}$. Because the reaction is fast, $k \approx 10^{13}$ cm$^3$ mol$^{-1}$ s$^{-1}$, tunneling contributions can be neglected. In Figure 5 the present value of $k_1$ is compared with the only other literature determination, the QRRK estimate for the reverse reaction by Bozzelli and co-workers.[7] The two rate constants are seen to be in agreement within a factor of 2 in the investigated temperature range.

**$SO_3$ + OH Reaction.** Computational results for an adduct formed between OH and $SO_3$ were reported by Wang et al.[26] and Wang and Hou.[35] Our similar computed structure is shown in Figure 1. We derive a binding enthalpy $D_0(HO-SO_3) = 120.1$ kJ mol$^{-1}$. This implies $\Delta_f H_0(HO-SO_3) = -473.0$ kJ mol$^{-1}$. Under atmospheric conditions this addition path could be a loss process for $SO_3$. However, in flames the adduct is insufficiently stable to be a sink for $SO_3$. For example, at 800 K the calculated equilibrium constant for $OH + SO_3 \rightleftharpoons HSO_4$ is $K_c = 1.5 \times 10^6$ cm$^3$ mol$^{-1}$. With a conservative upper limit for [OH] of $10^{-8}$ mol cm$^{-3}$, then on the assumption that $[SO_3] < [OH]$, the equilibrium fraction of $SO_3$ bound as adduct is less than 2%. At higher temperatures and/or lower [OH], an even smaller fraction of the $SO_3$ will be bound at equilibrium.

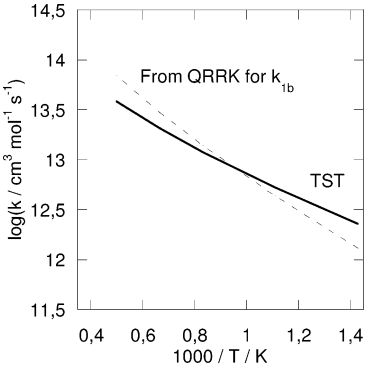


**Figure 5.** Arrhenius plot for the $SO_3 + H$ reaction. Dashed line: the rate constant derived from the QRRK estimate for the reverse reaction by Glarborg et al.[7] Solid line: TST rate constant from the present work.

A small concentration of $HOSO_3$ could be significant if it rapidly reacts to new products before decomposing thermally back to $OH + SO_3$. In contrast to the analogous $OH + SO_2$ adduct, which reacts readily with $O_2$, the thermochemistry for $O_2 + HOSO_3 \rightarrow HO_2 + SO_4$ is unfavorable. The latest $\Delta_f H_0(HO_2) = 15.2 \pm 0.3$ kJ mol$^{-1}$ [36] implies $\Delta_r H_0 = 231$ kJ mol$^{-1}$ for $HO_2$ formation. O atom elimination from $HOSO_3$ is predicted to be endothermic by 349 kJ mol$^{-1}$ and can therefore be ignored. We have not found a reaction path for elimination of $O_2$. Wang and Hou[35] assigned a transition state for elimination of $HO_2$ from $HOSO_3$ but our own investigations, including following the intrinsic reaction coordinate, suggest instead this TS (labeled TS6 in Figure 1) corresponds to direct abstraction by OH from $SO_3$. TS6 for direct abstraction lies 120.0 kJ mol$^{-1}$ above $OH + SO_3$ and the corresponding rate constant for $HO_2 + SO_2$ formation is summarized over 800−2000 K as $4.8 \times 10^4 T^{2.46} \exp(-114.1 \text{ kJ mol}^{-1}/RT)$ cm$^3$ mol$^{-1}$ s$^{-1}$.

## Detailed Kinetic Model

The revised rate constants for the $SO_3 + H$ (1), $SO_3 + O$ (2), and $SO_3 + OH$ (3) reactions were implemented in a detailed chemical kinetic model for high-temperature sulfur chemistry, drawn largely from recent work by the authors.[12,17] The reaction mechanism consists of a $H_2/O_2$ subset and a full description of the H/S/O reaction system. The mechanism contains the elementary steps that could conceivably influence the $SO_2/SO_3$ ratio at high temperatures. The sulfur oxides subset of the mechanism is listed in Table 3. The formation of $SO_3$ may proceed by a direct oxidation of $SO_2$,

$$SO_2 + O(+M) \rightleftharpoons SO_3(+M) \quad (4)$$

$$SO_2 + OH \rightleftharpoons SO_3 + H \quad (1b)$$

$$SO_2 + O_2 \rightleftharpoons SO_3 + O \quad (2b)$$

$$SO_2 + HO_2 \rightleftharpoons SO_3 + OH \quad (3b)$$

or it may involve $HOSO_2$ as an intermediate,

$$SO_2 + OH(+M) \rightleftharpoons HOSO_2(+M) \quad (5)$$

$$HOSO_2(+M) \rightleftharpoons SO_3 + H(+M) \quad (7)$$

$$HOSO_2 + O \rightleftharpoons SO_3 + OH \quad (9)$$

$$HOSO_2 + OH \rightleftharpoons SO_3 + H_2O \quad (10)$$

$$HOSO_2 + O_2 \rightleftharpoons SO_3 + HO_2 \quad (11)$$

The destruction of $SO_3$ may occur by

$$SO_3(+M) \rightleftharpoons SO_2 + O(+M) \quad (4b)$$

$$SO_3 + H \rightleftharpoons SO_2 + OH \quad (1)$$

$$SO_3 + O \rightleftharpoons SO_2 + O_2 \quad (2)$$

$$SO_3 + OH \rightleftharpoons SO_2 + HO_2 \quad (3)$$

$$SO_3 + HO_2 \rightleftharpoons HOSO_2 + O_2 \quad (5b)$$

$$SO_3 + SO \rightleftharpoons SO_2 + SO_2 \quad (6b)$$

Most of the reactions and rate constants have been discussed in some detail in previous work.[7,10−12,16,17] In addition to $k_1$, $k_2$, and $k_3$, only one rate constant has been modified in the present work. For the $SO_2 + SO_2$ reaction (6), we use an estimate, based on batch reactor results on $SO_2 + O_2$,[31] discussed below, and shock tube results on $SO_2$ decomposition.[37] Both studies indicate a reaction with a high activation energy, in the range 275−315 kJ/mol.

**TABLE 3: Rate Coefficients for Key Reactions in the Reaction Mechanism (Units: cm, mol, s, K)**

| no. | reaction | *A* | *n* | *E*/*R* | ref |
|---|---|---|---|---|---|
| 1 | $SO_3 + H \rightleftharpoons SO_2 + OH$ | 8.4E09 | 1.22 | 1670 | pw |
| 2 | $SO_3 + O \rightleftharpoons SO_2 + O_2$ | 2.8E04 | 2.57 | 14700 | pw |
| 3 | $SO_3 + OH \rightleftharpoons SO_2 + HO_2$ | 4.8E04 | 2.46 | 13700 | pw |
| 4 | $SO_2 + O(+M) \rightleftharpoons SO_3(+M)$[a] | 3.7E11 | 0.00 | 850 | 11 |
| | low-pressure limit | 2.4E27 | −3.60 | 2610 | |
| | Troe parameters 0.442, 316, 7442 | | | | |
| | low-pressure limit ($N_2$) | 2.9E27 | −3.58 | 2620 | 12 |
| | Troe parameters ($N_2$) 0.43, 371, 7442 | | | | |
| 5 | $SO_2 + OH(+M) \rightleftharpoons HOSO_2(+M)$[b] | 5.7E12 | −0.27 | 0 | 34 |
| | low-pressure limit | 1.7E27 | −4.09 | 0 | |
| | Troe parameters 0.10, 1E−30, 1E30 | | | | |
| 6 | $SO_2 + SO_2 \rightleftharpoons SO_3 + SO$ | 5.0E07 | 2.00 | 37750 | 37, est |
| 7 | $HOSO_2 \rightleftharpoons SO_3 + H$ | 1.4E18 | −2.91 | 27630 | 7, 1 atm |
| 8. | $HOSO_2 + H \rightleftharpoons SO_2 + H_2O$ | 1.0E12 | 0.00 | 0 | 7 |
| 9. | $HOSO_2 + O \rightleftharpoons SO_3 + OH$ | 5.0E12 | 0.00 | 0 | 7 |
| 10. | $HOSO_2 + OH \rightleftharpoons SO_3 + H_2O$ | 1.0E12 | 0.00 | 0 | 7 |
| 11. | $HOSO_2 + O_2 \rightleftharpoons HO_2 + SO_3$ | 7.8E11 | 0.00 | 330 | 38 |

[a] Enhanced third-body coefficients: $N_2 = 0$, $SO_2 = 10$, $H_2O = 10$.
[b] Enhanced third-body coefficients: $N_2 = 1$, $SO_2 = 5$, $H_2O = 5$.

## Modeling Results and Discussion

Predictions with the detailed chemical kinetic mechanism were compared with experimental results from the literature on oxidation of $SO_2$ to $SO_3$. The purpose of the modeling part has been to evaluate whether the novel values of $k_1$, $k_2$, and $k_3$ are consistent with the available experimental results and to discuss the implications. Results from batch reactors and flow reactors (assuming plug flow) were modeled with SENKIN,[39] which is part of the CHEMKIN library.[40] SENKIN performs an integration in time. The results of the SENKIN calculations were compared to flow reactor data using the nominal residence time in the isothermal part of the reactor.

The experimental data on $SO_3$ formation from $SO_2$ include results from premixed flames,[18−22] batch reactors,[31] and flow reactors.[7,23,43] The flame results have consistently been interpreted in terms of a fast rate constant for the $SO_3 + O$ reaction (2). On the basis of a more accurate value of $k_4$, the authors[12] recently reanalyzed the results of Smith and co-workers[21,22] and Merryman and Levy[20] to obtain a value of $k_2' = 7.8 \times 10^{11} \exp(-3065/T)$ cm$^3$/(mol s), in support of the earlier estimates. The flame interpretations[12,20−22] were all based on the assumption that the $SO_3$ level resulted from a balance between formation by $SO_2 + O(+M)$ (4) and consumption by $SO_3 + O$ (2), i.e., that the $SO_3 + H$ and $SO_3 + OH$ reactions could be disregarded due to a high O/H ratio in these flames. The present work indicates that the $SO_3 + O$ reaction is too slow to be an important consumption step for $SO_3$, even at the high temperatures in flames.

For the flames of Smith and co-workers,[21,22] which contained only trace amounts of water vapor as a hydrogen source, as well as for the flame of Merryman and Levy,[20] we estimate from kinetic modeling an O/H ratio ≈100 at the location where $d[SO_3]/dt = 0$ (at 1269 K[12,21,22] and 1685 K,[20] respectively). According to the results of the present study $k_1/k_2 \approx 10^5$, indicating that the $SO_3 + H$ reaction (1), not $SO_3 + O$ (2), is the controlling $SO_3$ consumption reaction in these lean flames. This is supported by the fact that the ratio $k_1/k_2'$ is about the same order of magnitude, ≈100, as the estimated O/H ratio in these flames. This means that there is no conflict between the present estimate for $k_2$ and the flame results, even though the flame data have been used to support a much higher value for $k_2$ previously.

Support for a high value of $k_2$ came recently from work by the authors on thermal dissociation of $SO_3$ in a quartz flow reactor.[12] In this work, a sink for atomic oxygen was required to explain the experimental results, and the loss of O was attributed partly to reaction with $SO_3$ (2). This interpretation is in conflict with the present value of $k_2$. The most likely explanation is loss of O on the reactor surface, but more work is required to confirm this. Sulfur trioxide is known to absorb strongly on glass surfaces where it acts to promote recombination of atomic oxygen.[2,41,42]

There are only few results reported in literature on the oxidation of $SO_2$ by $O_2$ in the absence of combustibles. Cullis et al.[31] studied gaseous oxidation of $SO_2$ by $O_2$ in a silica batch reactor in the temperature range 1173−1323 K (the upper limit dictated by the position of equilibrium between $SO_2$ and $SO_3$). The conversion of reactants was detected by measuring the pressure change in the vessel. It was confirmed by changes in the surface to volume ratio that the reaction observed was essentially homogeneous. Cullis et al. did not use the data to derive rate coefficients, partly because of considerable scatter and partly because the mechanism of $SO_3$ formation was uncertain. Due to the fairly small conversion of $SO_2$ under the reaction conditions, rate measurements were difficult and not readily reproducible; however, the data obtained were average results of a large number of experiments.

Figures 6 and 7 compare the experimental results of Cullis et al.[31] to modeling predictions with the detailed mechanism. The data indicate that the reaction increases roughly linearly with the concentration of sulfur dioxide, but only slightly with the concentration of oxygen (Figure 6), and that it has a high activation energy, about 315 kcal/mol (Figure 7). Assuming the presence of trace amounts of water vapor (50 ppm), calculations

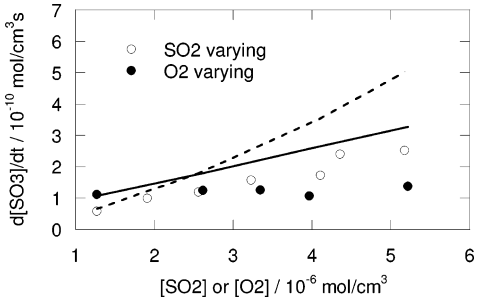


**Figure 6.** Comparison of experimental data[31] and modeling predictions for the $SO_3$ formation rate in a quartz batch reactor at a temperature of 1223 K and varying concentrations of $SO_2$ and $O_2$. In the modeling, trace amounts of water vapor (50 ppm) have been assumed to be present. Experimental data are shown as symbols; modeling predictions, as solid ($O_2$ varying) or dashed ($SO_2$ varying) lines.

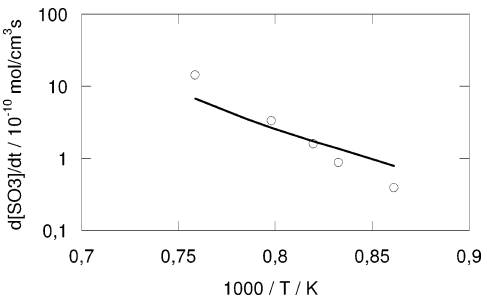


**Figure 7.** Comparison of experimental data[31] and modeling predictions for the $SO_3$ formation rate in a quartz batch reactor for $[SO_2] = [O_2] = 2.6 \times 10^{-6}$ mol cm$^{-3}$ and varying temperature. In the modeling, trace amounts of water vapor (50 ppm) have been assumed to be present. Experimental data are shown as symbols, modeling predictions as lines.

indicate that $SO_3$ is formed mainly by the sequence

$$SO_2 + OH(+M) \rightarrow HOSO_2(+M) \quad (4)$$

$$HOSO_2 + O_2 \rightarrow SO_3 + HO_2 \quad (11)$$

$$SO_2 + HO_2 \rightarrow SO_3 + OH \quad (5)$$

As the temperature increases, the sequence $SO_2 + SO_2 \rightarrow SO_3 + SO$ (6), $SO + O_2 \rightarrow SO_2 + O$, $SO_2 + O + M \rightarrow SO_3 + M$ (4) becomes more important. The modeling predictions are probably in agreement with the batch reactor results within the experimental uncertainty (Figures 6 and 7), but the mechanism of $SO_3$ formation under these conditions is still in question.

According to our modeling, the reaction sequence, $SO_2 + O_2 \rightarrow SO_3 + O$ (2b), $SO_2 + O(+M) \rightarrow SO_3(+M)$ (4), is not important for the $SO_3$ formation. However, the batch reactor data can be used to obtain an upper limit for $k_2$. Assuming that O is in steady state, we obtain $d[SO_3]/dt = 2k_{2b}[SO_2][O_2]$. From this equation, an upper limit of 14 cm$^3$ mol$^{-1}$ s$^{-1}$ can be derived for $k_{2b}$ at 1223 K, corresponding to $k_2(1223\ K) \leq 1.6 \times 10^9$ cm$^3$/(mol s) (Figure 3).

Experiments on oxidation of $SO_2$ to $SO_3$ by $O_2$ under flow reactor conditions have been reported by Flint and Lindsay,[43] Burdett et al.,[23] and Jørgensen et al.[44] These studies were all conducted at atmospheric pressure in electrically heated laminar flow reactors made of quartz or silica. In the present work the data from Flint and Lindsay and from Jørgensen et al. are selected for model validation; the results from Burdett et al. suffer from uncertainty in the reactor temperature profile.

Figure 8 compares modeling predictions with the data of Flint and Lindsay.[43] Their experiments were conducted with 1400 ppm $SO_2$ and 8% $H_2O$ in air at temperatures between 573 and

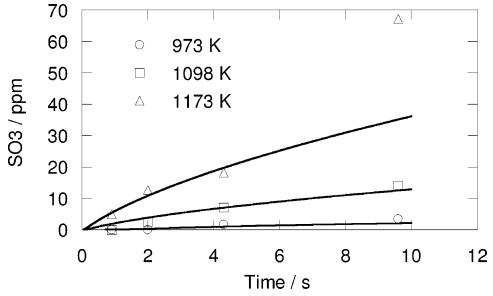


**Figure 8.** Comparison of experimental data[43] and modeling predictions for $SO_3$ formation in a quartz reactor at temperatures of 973−1173 K and atmospheric pressure. The quartz tube was 185 cm long and 1.6 cm internal diameter ($S/V = 1.3$ cm$^{-1}$). The inlet gases contained 0.14% $SO_2$, 8% $H_2O$, and air to balance. Symbols denote experimental results; solid lines denote modeling predictions.

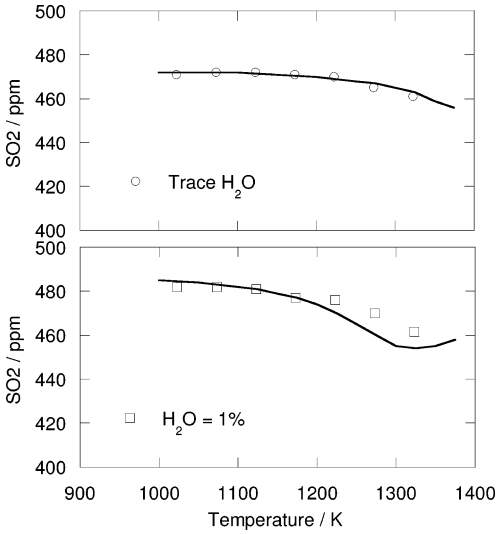


**Figure 9.** Comparison of experimental data[44] and modeling predictions for $SO_2$ oxidation in a quartz reactor at temperatures of 1023−1323 K and atmospheric pressure. The isothermal zone was 40 cm long and the reactor had a 3.15 cm internal diameter ($S/V = 0.6$ cm$^{-1}$). The inlet gas compositions were 472 ppm $SO_2$, 60% $O_2$, trace $H_2O$ (assumed 200 ppm), and $N_2$ to balance (upper figure); 485 ppm $SO_2$, 60% $O_2$, 1% $H_2O$, and $N_2$ to balance (lower figure). The residence time as a function of temperature is 5380[K]/*T*. Symbols denote experimental results; solid lines denote modeling predictions.

1173 K. Formation of $SO_3$ was detected only at 973 K and above. Except for a single data point, the modeling predictions are in good agreement with the flow reactor data. Flint and Lindsay attributed the $SO_3$ formation to the influence of catalysis by silica, but the present work indicates that it is largely a homogeneous reaction.

Figure 9 compares modeling predictions with the data of Jørgensen et al.[44] These experiments were conducted with about 480 ppm $SO_2$, 60% $O_2$, water vapor (trace amounts or 1%) in $N_2$ at temperatures between 1023 and 1323 K. Again the modeling predictions are in good agreement with the experimental results, under both semidry and moist conditions. At the highest temperatures in the moist set, the $SO_3$ concentration becomes limited by thermal equilibrium and the predicted $SO_2$ level increases.

Rate of production and sensitivity analysis indicate that the key reactions in $SO_3$ formation are $SO_2 + OH(+M) \rightarrow HOSO_2(+M)$ (5), $HOSO_2 + O_2 \rightarrow HO_2 + SO_3$ (11), and to a lesser extent $SO_2 + HO_2 \rightarrow SO_3 + OH$ (3b) and $SO_2 + OH \rightleftharpoons SO_3 + H$ (1b). Modeling predictions with the high rate constant for the $SO_3 + O$ reaction (2) derived from flames[12,20−22] lead

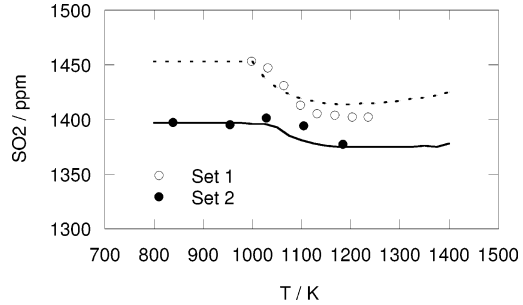


**Figure 10.** Comparison of experimental data[7] and modeling predictions for conversion of $SO_2$ as function of temperature during moist CO oxidation in a quartz flow reactor. Experimental data are shown as symbols; modeling predictions, as lines. Data set 1: 448 ppm CO, 1453 ppm $SO_2$, 4.3% $O_2$, and 1% $H_2O$, residence time as a function of temperature 243[K]/*T*. Data set 2: 446 ppm CO, 1395 ppm $SO_2$, 4.1% $O_2$, and 8.7% $H_2O$, residence time as a function of temperature 244[K]/*T*.

to a significant overprediction of the $SO_3$ formation rate through the inverse step, $SO_2 + O_2 \rightarrow SO_3 + O$ (2b), under the conditions of Figures 8 and 9. This is in support of the low value of $k_2$ estimated in the present work.

The experiments discussed above[23,31,43,44] were all conducted in the absence of combustibles. Radical formation from combustion has been shown to enhance the $SO_2$ oxidation rate significantly.[45] Glarborg et al.[7] studied $SO_2$ conversion during moist CO oxidation. The experiments were conducted using a quartz flow reactor, designed to approximate plug flow. It was placed in a three-zone electrically heated oven, allowing a uniform temperature profile with an uncertainty of ±10 K over the reactor length. The reactants CO, $SO_2$, $O_2$, and $H_2O$ were heated separately and mixed in a crossflow at the reactor inlet. The product gas was quenched at the exit of the reactor with cooling air and dried prior to analysis.

The experimental data are compared with modeling predictions in Figure 10. The agreement is within the experimental uncertainty. Compared to conditions in the absence of combustibles, the enhanced radical levels open up new pathways to formation and consumption of $SO_3$. The dominating $SO_3$ formation reaction is now recombination of $SO_2$ with atomic O,

$$SO_2 + O(+M) \rightarrow SO_3(+M) \quad (4)$$

and $SO_3$ decomposition proceeds mainly by the reactions

$$SO_3 + HO_2 \rightarrow HOSO_2 + O_2 \quad (11b)$$

$$HOSO_2(+M) \rightarrow SO_2 + OH(+M) \quad (5b)$$

$$SO_3 + H \rightarrow SO_2 + OH \quad (1)$$

It is noteworthy that although reactions 5 and 11 are important for $SO_3$ formation in moist $SO_2/O_2$ systems, they proceed in the reverse direction (11b, 5b) at higher radical levels and serve to consume $SO_3$.

Although the revised rate constant for the $SO_3 + H$ reaction (1) has only a small impact compared to earlier modeling for the $SO_2/SO_3$ ratio in combustion, the updated value for the $SO_3 + O$ reaction (2) has important implications. This reaction has been assumed to be an important consumption step for $SO_3$ in flames[18−22] and in flow reactor experiments,[7,10] whereas the reverse step between $SO_2$ and $O_2$ (2b) has been believed to contribute to $SO_3$ formation in $SO_2/O_2$ systems.[6,23] The present analysis indicate that reaction 2 is too slow to be important in any of these systems and that the observed $SO_3$ consumption must be attributed to other reactions, primarily $SO_3 + H$ (1). Also the $SO_3 + OH$ reaction (3) is generally too slow to be significant, but the reverse step between $SO_2$ and $HO_2$ (3b) may contribute to $SO_3$ formation under conditions with low radical levels.

## Conclusions

In the present study, ab initio calculations were carried out to estimate rate constants for the reactions of $SO_3$ with H, O, and OH at high temperatures. The $SO_3 + H \rightarrow SO_2 + OH$ reaction (1) is fast, with $k_1 = 8.4 \times 10^9 T^{1.22} \exp(-13.9 \text{ kJ mol}^{-1}/RT)$ cm$^3$ mol$^{-1}$ s$^{-1}$. Contrary to reaction 1, the reactions of $SO_3$ with O (2) and OH (3) appear to be quite slow due to high barriers to reaction, $k_2 = 2.8 \times 10^4 T^{2.57} \exp(-122.3 \text{ kJ mol}^{-1}/RT)$ and $k_3 = 4.8 \times 10^4 T^{2.46} \exp(-114.1 \text{ kJ mol}^{-1}/RT)$ cm$^3$ mol$^{-1}$ s$^{-1}$. Modeling predictions with a revised reaction mechanism for $SO_2/SO_3$ chemistry are in good agreement with a range of experimental data from reactor experiments. The calculations indicate that oxidation of $SO_2$ to $SO_3$ with and without presence of combustibles involve primarily recombination of $SO_2$ with O and OH radicals. Reaction 1 may limit the $SO_3$ concentration, and reactions 2 and 3 are unimportant for the $SO_2/SO_3$ ratio under most conditions of interest.

**Acknowledgment.** We acknowledge support from the CHEC (Combustion and Harmful Emission Control) Research Program, PSO-Elkraft (Grant FU-2207), the Robert A. Welch Foundation (Grant B-1174) and the UNT Faculty Research Fund. A three month guest professorship for P.M. at DTU was funded by the Otto Mønsted Fund. Computer facilities were provided at the National Center for Supercomputing Applications (Grant CHE000015N), at the Research Cluster operated by UNT Academic Computing Services, and purchased with funding from the National Science Foundation (Grant CHE-0342824).

## References and Notes

(1) Miller, J. A.; Klippenstein, S. J. *J. Phys. Chem. A* **2006**, *110*, 10528−10544.
(2) Cullis, C. F.; Mulcahy, M. F. R. *Combust. Flame* **1972**, *18*, 225−292.
(3) Srivastava, R. K.; Miller, C. A.; Erickson, C.; Jambhekar, R. *J. Air Waste Manage. Assoc.* **2004**, *54*, 750−762.
(4) Christensen, K. A.; Livbjerg, H. *Aerosol Sci. Technol.* **1996**, *25*, 185−199.
(5) Jensen, J. R.; Nielsen, L. B.; Schultz-Møller, C.; Wedel, S.; Livbjerg, H. *Aerosol Sci. Technol.* **2000**, *33*, 490−509.
(6) Glarborg, P.; Marshall, P. *Combust. Flame* **2005**, *141*, 22−38.
(7) Glarborg, P.; Kubel, D.; Dam−Johansen, K.; Chiang, H. M.; Bozzelli, J. W. *Int. J. Chem. Kinet.* **1996**, *28*, 773−790.
(8) Johnsson, J. E.; Glarborg, P. Sulfur Chemistry in Combustion I − Sulfur in Fuels and Combustion Chemistry. *Pollutants from Combustion. Formation Mechanisms and Impact on Atmospheric Chemistry*; Vovelle, C., Ed.; Kluwer Academic Publisher: Dordrecht, The Netherlands, 2000; pp 283−301.
(9) Mueller, M. A.; Yetter, R. A.; Dryer, F. L. *Int. J. Chem. Kinet.* **2000**, *32*, 317−339.
(10) Alzueta, M. U.; Bilbao, R.; Glarborg, P. *Combust. Flame* **2001**, *127*, 2234−2251.
(11) Naidoo, J.; Goumri, A.; Marshall, P. *Proc. Combust. Inst.* **2005**, *30*, 1219−1225.
(12) Yilmaz, A.; Hindiyarti, L.; Jensen, A. D.; Glarborg, P.; Marshall, P. *J. Phys. Chem. A* **2006**, *110*, 6654−6659.
(13) Frenklach, M.; Lee, J. H.; White, J. N.; Gardiner, W. C., Jr. *Combust. Flame* **1981**, *41*, 1−16.
(14) Cerru, F. G.; Kronenburg, A.; Lindstedt, R. P. *Proc. Combust. Inst.* **2005**, *30*, 1227−1235.
(15) Cerru, F. G.; Kronenburg, A.; Lindstedt, R. P. *Combust. Flame* **2006**, *146*, 437−455.
(16) Dagaut, P.; Lecomte, F.; Mieritz, J.; Glarborg, P. *Int. J. Chem. Kinet.* **2003**, *35*, 564−575.

(17) Rasmussen, C. L.; Glarborg, P.; Marshall, P. *Proc. Combust. Inst.* **2007**, *31*, 339−347.
(18) Fenimore, C. P.; Jones, G. W. *J. Phys. Chem.* **1965**, *69*, 3593.
(19) Schofield, K. *J. Phys. Chem. Ref. Data* **1973**, *2*, 25−84.
(20) Merryman, E. L.; Levy, A. *Proc. Combust. Inst.* **1979**, *17*, 727−736.
(21) Smith, O. I.; Tseregounis, S.; Wang, S.-N. *Int. J. Chem. Kinet.* **1982**, *14*, 679−697.
(22) Smith, O. I.; Tseregounis, S.; Wang, S.-N.; Westbrook, C. K. *Combust. Sci. Technol.* **1983**, *30*, 241−271.
(23) Burdett, N. A.; Langdon, W. E.; Squires, R. T. *J. Inst. Energy* **1984** September, 373.
(24) Montgomery, J. A., Jr.; Frisch, M. J.; Ochterski, J. W.; Petersson, G. A. *J. Chem. Phys.* **1999**, *110*, 2822.
(25) McKee, M. L. *J. Am. Chem. Soc.* **1993**, *115*, 9136.
(26) Wang, X.-B.; Nicholas, J. B.; Wang, L.-S. *J. Phys. Chem. A* **2000**, *104*, 504.
(27) *NIST-JANAF Thermochemical Tables*, 4th ed.; Chase, M. W., Jr., Ed.; American Chemical Society and the American Institute of Physics: Woodbury, NY, 1998.
(28) Westenberg, A. A.; deHaas, N. J. *J. Chem. Phys.* **1975**, *62*, 725.
(29) Dunning, T. H., Jr.; Peterson, K. A.; Wilson, A. K. *J. Chem. Phys.* **2001**, *114*, 9244.
(30) Yamaguchi, K.; Jensen, F.; Dorigo, A.; Houk, K. N. *Chem. Phys. Lett.* **1988**, *149*, 537.
(31) Cullis, C. F.; Henson, R. M.; Trimm, D. L. *Proc. R. Soc. A* **1966**, *295*, 72−83.
(32) Goumri, A.; Roucha, J. D.-R. Laakso, D.; Smith, C. E.; Marshall, P. *J. Phys. Chem. A* **1999**, *103*, 11328.
(33) Joens, J. A. *J. Phys. Chem. A* **2001**, *105*, 11041.
(34) Blitz, M. A.; Hughes, K. J.; Pilling, M. J. *J. Phys. Chem. A* **2003**, *107*, 1971−1978.
(35) Wang, B.; Hou, H. *Chem. Phys. Lett.* **2005**, *410*, 235−241.
(36) Ruscic, B.; Pinzon, R. E.; Morton, M. L.; Srinivasan, N. K.; Su, M.-C.; Sutherland, J. W.; Michael, J. V. *J. Phys. Chem. A* **2006**, *110*, 6592−6601.
(37) Raju, M. T.; Babu, S. V.; Rao, V. S. *Chem. Phys.* **1980**, *48*, 411−416.
(38) Atkinson, R.; Baulch, D. L.; Cox, R. A.; Hampson, R. F.; Kerr, J. A.; Troe, J. *J. Phys. Chem. Ref. Data* **1992**, *21*, 1125−1568.
(39) Lutz, A.; Kee, R. J.; Miller, J. A. SENKIN: A Fortran Program for Predicting Homogenous Gas Phase Chemical Kinetics with Sensitivity Analysis. Sandia Report SAND87-8248; Sandia National Laboratories: Livermore, CA, 1987.
(40) Kee, R. J.; Rupley, F. M.; Miller, J. A. CHEMKIN−II: A Fortran Chemical Kinetics Package for the Analysis of Gas-Phase Chemical Kinetics. Sandia Report SAND89-8009; Sandia National Laboratories: Livermore, CA, 1989.
(41) Kaufman, F. *Proc. R. Soc. London, A* **1958**, *247*, 123.
(42) Mulcahy, M. F. R.; Stevens, J. R.; Ward, J. C.; Williams, D. J. *Proc. Combust. Inst.* **1969**, *12*, 323.
(43) Flint, D. Lindsay, A. W. *Fuel* **1952**, *30*, 288.
(44) Jørgensen, T. L.; Livbjerg, H.; Glarborg, P. Homogeneous and heterogeneously catalyzed oxidation of $SO_2$, submitted for publication.
(45) Glarborg, P. *Proc. Combust. Inst.* **2007**, *31*, 77−98.